

## Non-equilibrium growth of a binary alloy

A.C. FOWLER\*

MACSI, University of Limerick, Limerick, Ireland

OCIAM, University of Oxford, Oxford, UK

\*Corresponding author: [fowler@maths.ox.ac.uk](mailto:fowler@maths.ox.ac.uk)

[Received on 26 June 2021; revised on 13 February 2022; accepted on 19 April 2022]

We present an interpretation of the phase diagram for a binary alloy from the point of view of reaction dynamics. We consider a model system in which the two-component liquid phase is an ideal solution, but the solid phase can be non-ideal, with its non-ideality increasing with reducing temperature. We show how a ‘batch’ model for the evolution of the two-component solid–liquid system, in which the interfacial growth rates are proportional to free energy differences, leads to a set of four differential equations, whose equilibria correspond to the familiar solidus and liquidus curves. In addition, we explain how the transitions between them depend on the bifurcation structure of the solutions. We show that locally stable mixed-phase solutions can exist below the eutectic temperature, thus providing an alternative explanation for the observation of super-cooled liquids, and we also explain why complete solidification ‘normally’ occurs below the eutectic temperature, despite the fact that this temperature has no intrinsic dynamic significance, being simply a value at which two completely different equilibrium states happen to share a common liquid concentration.

**Keywords:** phase diagram; non-equilibrium growth; binary alloy.

### 1. Introduction

Phase diagrams, such as that shown in Fig. 1, are commonly encountered in materials science (e.g. Flemings 1974) and petrology (e.g. Morse 1980). In metallurgical contexts they often concern two-component metal mixtures, referred to as alloys, for example that of lead–tin; in petrology, they are of concern in the melting of polycrystalline rocks, or in the crystallization of multicomponent magmas such as basalt, where a sequence of crystals such as olivine, plagioclase and pyroxene may sequentially be precipitated from the melt. The chemistry of rock and magma is a dauntingly complex subject (a simplified summary from a theoretical perspective can be found in Fowler (2011, chapter 9)), commonly involving three or more components, but in the present case we will restrict ourselves to alloys (or magmas) of two components.

Figure 1 requires some explanation. It portrays three distinct curves, labelled L for liquidus, S for solidus and V for solvus, relating temperature  $T$  to concentration of one component in a two-component mixture, coloured respectively blue, black and green. The curves are truncated by the horizontal pink line through the point E, which is known as the eutectic point, where the two branches of the liquidus curve meet. As we shall see below, while the curves appear as distinct segments, they are actually continuous, with the missing sections cut off by the pink line.

Above the liquidus curves, the mixture exists as a liquid. If (at a fixed concentration) the temperature is reduced to the liquidus curve, then solid begins to form, but not at the same concentration. In fact the forming solid has a composition on the solidus curve next to the liquidus at the same temperature. Further cooling causes the liquid concentration to remain on the liquidus, and the forming solid follows the concentration on the solidus. This carries on till the temperature reaches the eutectic temperature, when now solid can form at the concentration on either solidus, and the liquid concentration can

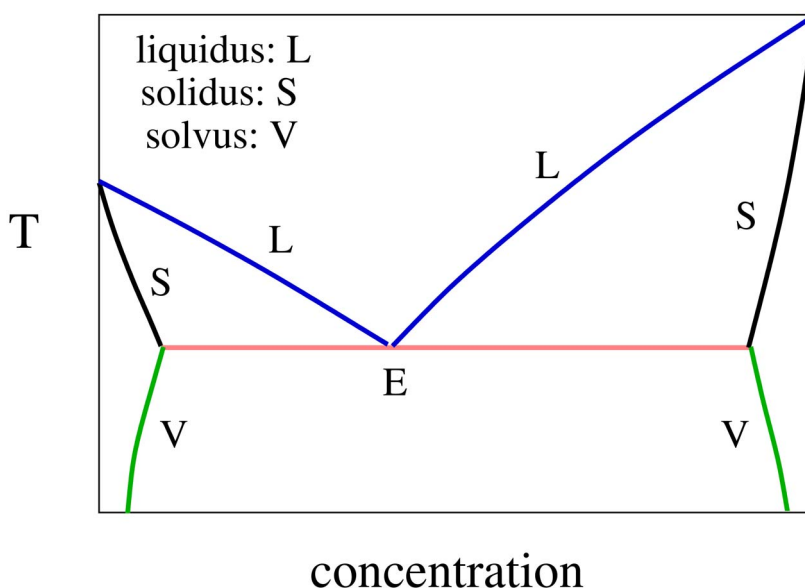


FIG. 1. A typical eutectic phase diagram for a binary alloy, which represents equilibrium concentration of one component when either solid and liquid coexist (the liquidus is the liquid concentration, the solidus is the corresponding solid concentration), or the mixture is completely solid, when the two branches of the solvus curve provide the two stable compositions of solid grains.

remain at the eutectic concentration. In thermodynamic equilibrium below the eutectic temperature, one conventionally supposes complete solidification has occurred, and the solvus curve(s) represent the stable concentrations of possible solid phases. This is called unmixing, and is the analogy for a solid of the familiar liquid unmixing of oil and water, for example.

Our interest in this is motivated by the paper by [Rudge \*et al.\* \(2011\)](#), who were interested in the non-equilibrium melting or crystallization of a multicomponent material. While that work was largely directed towards developing a computational strategy for melting in the Earth's mantle, our purpose here is to elaborate a mathematical understanding of the melting or solidification process. At least one reason for doing so is to provide a systematic framework for the consideration of the suggestion by [Maaløe \(1978\)](#) that non-equilibrium crystallization in the vicinity of a eutectic point could provide an explanation for the oscillatory zoning that is found in layered magmatic intrusions ([Wager and Brown 1968](#)). Non-equilibrium crystallization may be important in magmas, in particular, and is commonly represented empirically in terms of sub-cooling below the liquidus ([Dowty 1980](#)), but the description must be more complex near a eutectic point or cotectic line.

In order to expound our theory, it is necessary first to explain how a phase diagram such as that in [Fig. 1](#) comes about; this is done in [Section 2](#). The consequent non-equilibrium growth theory is then promoted in [Section 3](#). Discussion and conclusions follow.

## 2. Thermodynamic equilibrium

In a multicomponent mixture consisting of  $n$  components labelled with a suffix  $i$ , the chemical potential of the  $i$ -th component is

$$\mu_i = \mu_{i0} + RT \ln a_i, \quad (2.1)$$

where  $a_i$  is the activity,  $R$  is the gas constant,  $T$  is absolute temperature and the units are  $\text{J mole}^{-1}$ . For an ideal (or pure) substance,  $a_i = x_i$ , where  $x_i$  is the mole fraction of component  $i$ . The reference value  $\mu_{i0}$  is a function of temperature (and pressure, but that will be ignored here). The definition (2.1) applies in both solid and liquid phases, with different activities and reference values which will be denoted by superscripts  $S$  and  $L$ . The difference between solid and liquid chemical potentials for component  $i$  is then

$$\Delta\mu_i = \mu_i^S - \mu_i^L = RT \ln \left[ \frac{a_i^S}{a_i^L K_i} \right], \quad (2.2)$$

where

$$K_i(T) = \exp \left[ -\frac{\Delta\mu_{i0}}{RT} \right], \quad \Delta\mu_{i0} = \mu_{i0}^S - \mu_{i0}^L. \quad (2.3)$$

The condition for equilibrium at a (flat) interface is then

$$\Delta\mu_i = 0 \quad (2.4)$$

for each component  $i$ .

To be specific, we will label mole fractions in the liquid phase as  $x_i$ , and in the solid phase as  $y_i$ . In general, we will then have

$$a_i^S = a_i^S(\mathbf{y}), \quad a_i^L = a_i^L(\mathbf{x}). \quad (2.5)$$

In equilibrium we have  $\Delta\mu_i = 0$  for each  $i$ , and thus the  $n$  equations

$$a_i^S(\mathbf{y}) = a_i^L(\mathbf{x}) K_i(T); \quad (2.6)$$

for a given (liquidus) set of concentrations at a given temperature, these equations in principle determine the (possibly multiple) solidus concentrations. We now consider two examples; in the first we consider the case where the solid phases form a solid solution (i.e. the components are ideal), and in the second we consider non-ideal solid components. In both cases, we assume the liquid components are ideal and therefore mix (unlike oil and water, for example). We will also restrict ourselves in specific examples to binary mixtures in which there are two components.

### 2.1 Ideal solid solution

If the liquid components form an ideal solution, then

$$a_i^L = x_i, \quad (2.7)$$

and we assume this henceforth. It is commonly the case in aqueous solutions, though not always in magmas, for example. Suppose also that the solid solution is ideal; then

$$a_i^S = y_i. \quad (2.8)$$

What this means is that in forming the crystal lattice of the solid, the two components are interchangeable: there is no energy penalty to replacing one component atom (or molecule) with another. A particular geological example of this is the mineral olivine, which is a solid solution of forsterite ( $\text{Mg}_2\text{SiO}_4$ ) and fayalite ( $\text{Fe}_2\text{SiO}_4$ ), in which the magnesium and iron atoms are interchangeable.

**2.1.1 Pure component melting points.** If we consider a pure component  $i$  so that  $a_i^L = a_i^S = 1$ , then

$$\Delta\mu_i = \Delta\mu_{i0} = \mu_{i0}^S - \mu_{i0}^L = -RT \ln K_i. \quad (2.9)$$

Suppose the melting point is  $T_i$ ; then for  $T > T_i$  we must have  $\Delta\mu_{i0} > 0$  and for  $T < T_i$ ,  $\Delta\mu_{i0} < 0$ . In order to provide specific examples, we will suppose

$$\Delta\mu_{i0} = A_i R \left( \frac{T}{T_i} - 1 \right), \quad (2.10)$$

whence

$$K_i = \exp \left[ A_i \left( \frac{1}{T} - \frac{1}{T_i} \right) \right], \quad (2.11)$$

where the coefficients  $A_i$  are positive.

**2.1.2 Phase diagrams.** For an ideal solid solution, the phase diagram is determined by (2.6), which becomes

$$y_i = x_i K_i. \quad (2.12)$$

For a binary mixture in which we write  $x = x_2$ ,  $y = y_2$ , this gives the pair of equations

$$y = xK_2, \quad 1 - y = (1 - x)K_1. \quad (2.13)$$

These are easily solved to find

$$x = \frac{1 - K_1}{K_2 - K_1}, \quad y = K_2 x. \quad (2.14)$$

An example is plotted in Fig. 2, with parameters designed to make the figure similar to that of the albite–anorthite phase diagram (McBirney 1984), but note that the figure uses mole fraction as concentration rather than the more common mass fraction.

## 2.2 Non-ideal solid solutions

Next, we consider the case where the liquid phase is an ideal solution, but the solid phase is not. At this point we deviate from Rudge *et al.* (2011), who in their treatment assume ideal phases (two lines below

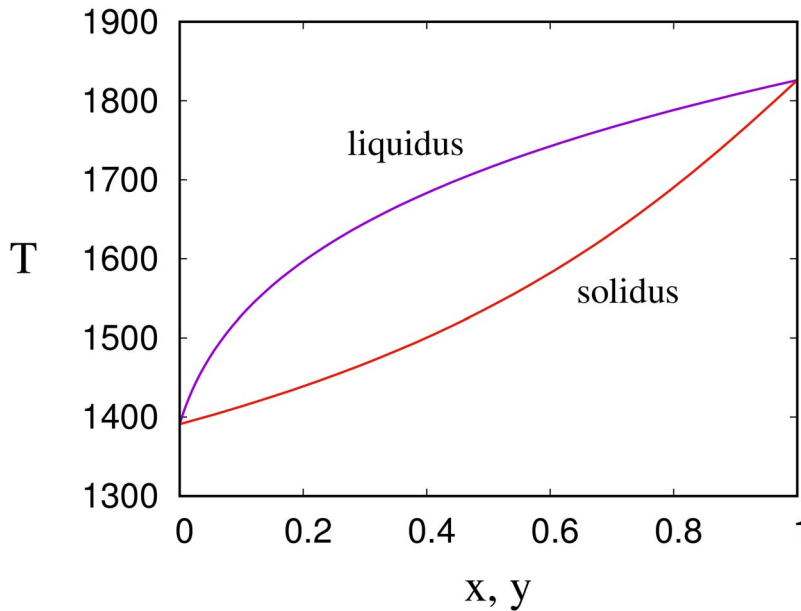


FIG. 2. A typical pair of solidus–liquidus curves (similar to that of albite–anorthite, see [McBirney \(1984, p. 196\)](#)), obtained from (2.14) and (2.11) using values  $T_1 = 1,391$  K,  $T_2 = 1,826$  K,  $A_1 = 6T_1$ ,  $A_2 = 8T_2$ . In this and following figures,  $x$  represents the liquidus concentration, and  $y$  the solidus concentration.

their equation (69)). We then have from (2.2), and for a binary mixture with  $x = x_2$ ,  $y = y_2$ ,

$$\Delta\mu_1 = RT \ln \left[ \frac{(1-y)\gamma_1}{(1-x)K_1} \right], \quad \Delta\mu_2 = RT \ln \left[ \frac{y\gamma_2}{xK_2} \right], \quad (2.15)$$

where  $\gamma_i$  are activity coefficients ( $a_i = \gamma_i y_i$ ) which are functions of  $y_i$ , and equal to one when  $y_i = 1$  (pure component  $i$ ). To be specific, we will take

$$\gamma_1 = \exp[\chi y^2], \quad \gamma_2 = \exp[\chi(1-y)^2], \quad (2.16)$$

which is an example of a [Margules \(1895\)](#) expression, and can be derived from statistical mechanical considerations (e.g. [Flory 1942](#)). We will take the unmixing coefficient  $\chi$  to be dependent on temperature in the form

$$\chi = 2 \exp \left[ A_V \left( \frac{1}{T} - \frac{1}{T_V} \right) \right], \quad (2.17)$$

where the limit of ideality is obtained for small  $T_V$ . Unmixing occurs for  $\chi > 2$ , i.e.  $T < T_V$ . There is no physics behind this choice, and the choice is by analogy with the choice for  $K_i$  in (2.11), and also to provide realistic looking solvus curves, as in [Fig. 3](#) below (or [Fig. 1](#)).

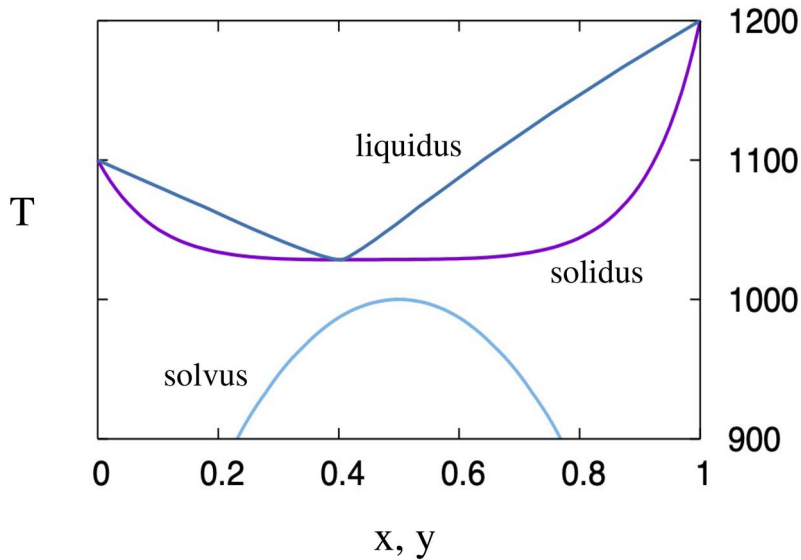


FIG. 3. A typical pair of solidus–liquidus curves in which the solid phase has mild unmixing. At lower temperatures the *solvus* curve indicates where unmixing of the solid phase occurs (see [McBirney \(1984, p. 94\)](#)). These curves are obtained from (2.18) and (2.22) using values  $T_1 = 1,100$  K,  $T_2 = 1,200$  K,  $A_1 = 5,000$  K,  $A_2 = 5,000$  K,  $A_V = 2,000$  K,  $T_V = 1,000$  K,  $H_{21} = 0$  K.

Equilibrium implies that  $\Delta\mu_i = 0$ , and thus

$$\gamma_2 y = x K_2(T), \quad (1-y)\gamma_1 = (1-x)K_1(T). \quad (2.18)$$

Elimination of  $x$  allows us to plot the solidus  $T = T_S(y)$  as the solution of the equation

$$G(y, T) = \frac{(1-y)\gamma_1}{K_1} + \frac{y\gamma_2}{K_2} = 1, \quad (2.19)$$

and then the liquidus is defined as

$$x_L = \frac{y\gamma_2}{K_2}. \quad (2.20)$$

The effect of the unmixing coefficient in the solid phase is to depress the liquidus and solidus curves until they may coincide at a eutectic point, as shown in [Fig. 3](#).

The unmixing in the solid phase means that for  $T < T_V$  the Gibbs free energy of the solid phase is a  $W$ -shaped function of the concentration, and this carries through to the pure solid phase. The Gibbs free energy of a presumed homogeneous solid phase is

$$G_S = (1-y)\mu_{10}^S + y\mu_{20}^S + RT[(1-y)\ln(1-y) + y\ln y + \chi y(1-y)], \quad (2.21)$$

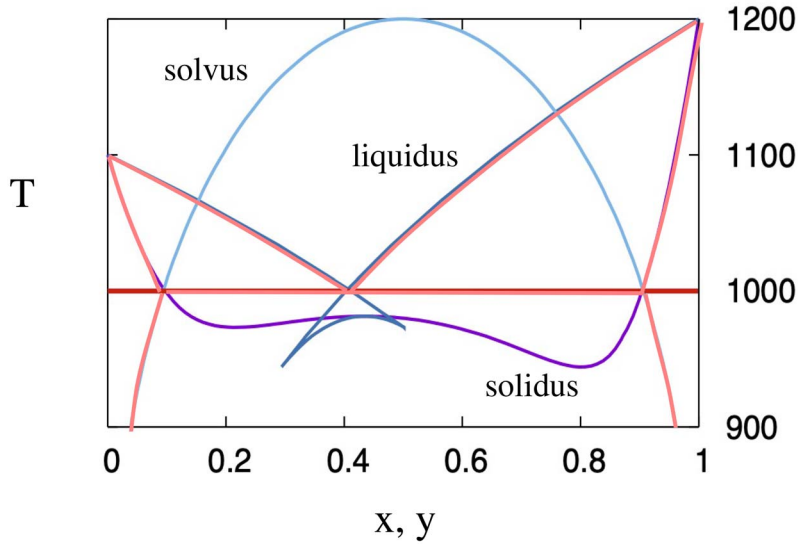


FIG. 4. A typical eutectic phase diagram, obtained as in Fig. 3, with the only change being that  $T_V = 1,200$  K. The solidus, liquidus and solvus curves are shown, together with a (red) horizontal line which appears to connect the eutectic point and the two solidus/solvus points. The usually viewed curves are outlined in pink.

which is  $W$ -shaped if  $\chi \gtrsim 2$ . In this case there are three turning points of  $G_S$ , of which the outer two (minima) provide the stable unmixed states. These are given by the zeroes of

$$H_S(y, T) = \frac{1}{RT} \frac{\partial G_S}{\partial y} = \frac{H_{21}}{T} + \ln \left( \frac{y}{1-y} \right) + \chi(1-2y), \quad H_{21} = \frac{\mu_{20}^S - \mu_{10}^S}{R}, \quad (2.22)$$

and the outer two zeroes of this are plotted in Fig. 3. They form a curve (with maximum at  $T \approx T_V$ ) called the *solvus*. Note that equivalently on this curve,  $\Delta\mu_1^S = \Delta\mu_2^S$ .

The effect of the unmixing coefficient in Fig. 3 can be seen to lower the liquidus and solidus curves so that they touch at a *eutectic point* (around  $x = y = 0.4$ ,  $T = 1,030$  K). Just below this temperature, the solid is an ideal solution in the sense that the Gibbs free energy  $G_S$  has a unique minimum (at  $y = 0.5$  in our illustration). However, when  $T$  decreases below  $T_V (= 1,000$  K in the figure),  $G_S$  becomes a double well potential, and unmixing occurs on the solvus, forming solid phases of two separate compositions (e.g.  $y = 0.2$  and  $0.8$  for  $T$  just below  $900$  K). The unmixing is commonly modelled using the Cahn–Hilliard equation (e.g. Cahn and Hilliard 1958, Kuhl and Schmid 2007).

**2.2.1 Eutectic phase diagram.** If the unmixing temperature  $T_V$  is higher, then we obtain the usual sort of eutectic phase diagram which we illustrated in Fig. 1. This is shown in Fig. 4, which is in fact the complete version of Fig. 1, that is to say it shows the complete forms of the equilibrium curves obtained by solving (2.19), (2.20) and (2.22), that is,

$$G(y, T) = 1, \quad x = x_L(y, T), \quad H_S(y, T) = 0, \quad (2.23)$$

which, respectively, define the solidus, liquidus and solvus. These curves are shown in Fig. 4, together with a red horizontal line which simply indicates the fact that the two intersection points of the solidus

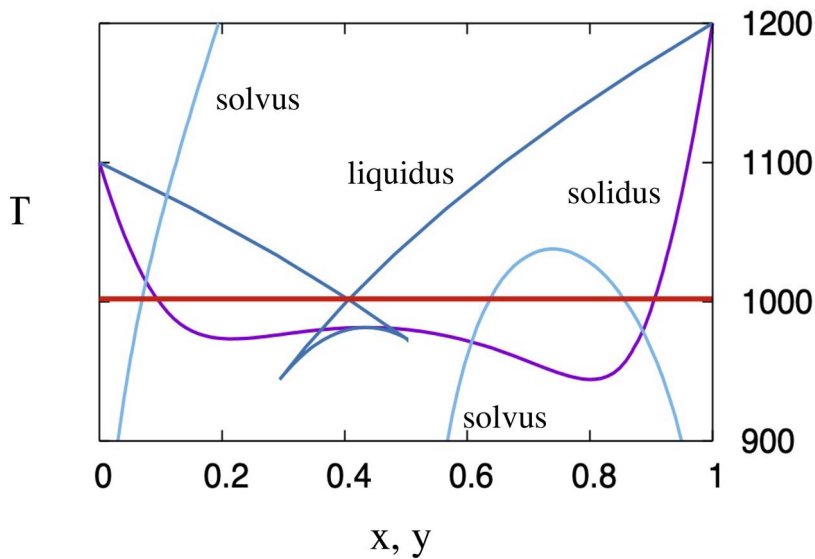


FIG. 5. The same solidus and liquidus curves as in Fig. 4, but now the solvus is plotted with  $H_{21} = 0.2$ . The resultant asymmetry breaks the symmetric pitchfork of the three stationary points of  $G_S$ , and their intersection with the solidus is no longer at the eutectic temperature.

and solvus, as well as the eutectic point, all appear to occur at the same temperature. The simplest way to show this is the case is to use the well-known fact that the solidus and liquidus curves for the phase free energies

$$G_L(x) = (1-x)\mu_1^L + x\mu_2^L, \quad G_S(y) = (1-y)\mu_1^S + y\mu_2^S \quad (2.24)$$

(the last is the same definition as in (2.21)) satisfy

$$\frac{\partial G_S}{\partial y} = \frac{\partial G_L}{\partial x} = \frac{G_S(y) - G_L(x)}{y - x} \quad (2.25)$$

at equilibrium, because, due to the symmetry in our choice of Margules unmixing coefficients (the same  $\chi$  in each free energy),

$$\frac{\partial G_S}{\partial y} = \mu_2^S - \mu_1^S, \quad \frac{\partial G_L}{\partial x} = \mu_2^L - \mu_1^L. \quad (2.26)$$

At the eutectic point, both chordal tangents to the  $U$ -shaped  $G_L$  and the  $W$ -shaped  $G_S$  are collinear, and they will coincide with the solvus precisely if the tangent slope is zero.  $G_L$  is symmetric, and  $G_S$  is symmetric if and only if  $H_{21} = 0$ , which is therefore the condition for the solvus/solidus intersection occurring at the eutectic temperature. Figure 5 shows an example in which the symmetry is broken in this fashion by having  $H_{21} \neq 0$ .

A comment should be made on the symmetry-breaking solvus in Fig. 5. The  $W$ -shaped  $G_S$  has in general three turning points for low enough  $T$ , and in Fig. 4 we omitted the central turning point (at



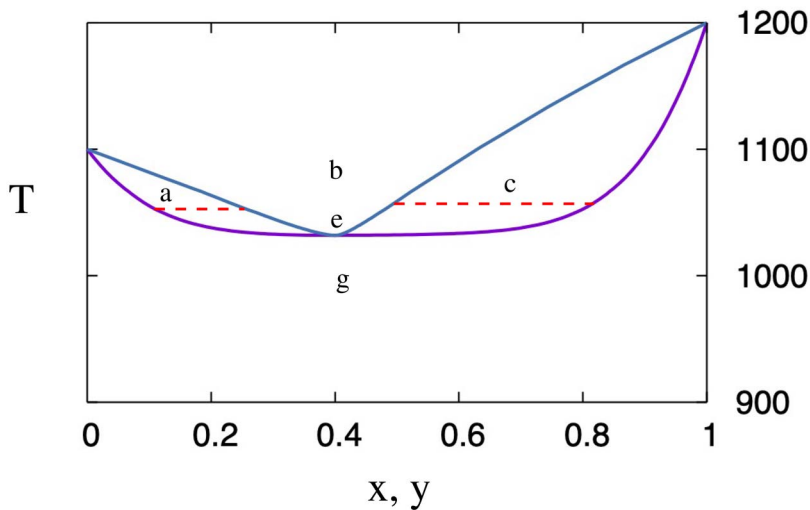


FIG. 6. The solidus and liquidus curves of Fig. 3. The letters refer to different starting conditions, as described in the text.

$y = 0.5$ ) where, for  $T < T_V$ ,  $G_S$  has a maximum. If this were re-inserted, the solvus would be a pitchfork (and indeed have a pitchfork bifurcation) as  $T$  reduces through  $T_V$ . The introduction of asymmetry by having  $H_{21} \neq 0$  in Fig. 5 causes the pitchfork to break, so that the left branch remains stable for all  $T$ , while the unstable middle branch disappears in a saddle-node bifurcation with the right branch at  $T \approx 1,030$  K. This asymmetry will, however, play no part in our discussion, because our model will describe only growth at solid/liquid interfaces, and not internal solid state evolution.

There are a number of interesting features in Figs 4 and 5. The normal phase diagram that one sees consists of the curves outlined in pink in Fig. 4, equivalent to Fig. 1. But we see from our discussion that the horizontal red line in Fig. 5 carries no intrinsic thermodynamic significance. Further, the liquidus and solidus curves both continue to temperatures below the eutectic temperature. Naturally, we presume that such states are not tenable, but there is nothing in the equilibrium conditions which can tell us this. It is for this reason that we now turn to a consideration of non-equilibrium crystal growth.

### 3. Non-equilibrium growth

Our discussion of non-equilibrium crystallization follows that of Rudge *et al.* (2011). However, our focus is different; we are here interested in the dynamical systems problem of understanding the bifurcation structure of the phase diagram. We begin our analysis with consideration of Fig. 6, which is simply Fig. 3 with the solvus curve omitted, as the solid unmixing plays an unimportant rôle, and will be ignored. We will obtain two ordinary differential equations for the liquid and solid concentrations  $x$  and  $y$ , in which  $T$  is a parameter, and then study the behaviour of trajectories in the  $(x, y)$  phase plane. Our first aim is to derive a coherent model for the evolution of  $x$  and  $y$ . Later, we will address the more complicated issue of describing fig 5.

We will follow the essential idea of Rudge *et al.* (2011) in writing macroscopic conservation laws for the constituents in each phase. For a binary mixture, this gives us four equations, two for each constituent in each phase. Because we are interested in the non-equilibrium kinetics of the precipitation/dissolution process, we will ignore transport terms on the basis that the volume under consideration is small, and that the concentrations are homogeneous.

First, we need to deal with the relation between mole fractions  $x_i$  and concentrations  $c_i$ , which are mass fractions. The relation is easily derived, and is given by [Rudge \*et al.\* \(2011\)](#), and is

$$c_i = \frac{M_i x_i}{M}, \quad x_i = \frac{M c_i}{M_i}, \quad M = \sum_j M_j x_j = \left( \sum_j \frac{c_j}{M_j} \right)^{-1}, \quad (3.1)$$

where  $M_j$  are the molecular weights of component  $i$ . In our binary case where the mole fractions of component 2 in liquid and solid are denoted  $x$  and  $y$ , respectively, we will denote the corresponding concentrations as  $c$  and  $s$ , respectively, and then we have

$$x = \frac{c}{M_2 \left( \frac{c}{M_2} + \frac{(1-c)}{M_1} \right)}, \quad y = \frac{s}{M_2 \left( \frac{s}{M_2} + \frac{(1-s)}{M_1} \right)}. \quad (3.2)$$

We will consider a volume  $V$  having porosity (liquid volume fraction)  $\phi$ , and liquid and solid concentrations  $c$  and  $s$ , as above. The four equations describing the kinetics of melting or crystallization are

$$\begin{aligned} \frac{\partial}{\partial t}(\rho_l \phi c V) &= \Sigma V \Gamma_2, \\ \frac{\partial}{\partial t}\{\rho_l \phi (1-c) V\} &= \Sigma V \Gamma_1, \\ \frac{\partial}{\partial t}\{\rho_s (1-\phi) s V\} &= -\Sigma V \Gamma_2, \\ \frac{\partial}{\partial t}\{\rho_s (1-\phi) (1-s) V\} &= -\Sigma V \Gamma_1. \end{aligned} \quad (3.3)$$

In these equations,  $\rho_s$  and  $\rho_l$  are the solid and liquid densities,  $\Sigma$  is the specific surface area, which we would generally take to be a function of  $\phi$ , and  $\Gamma_i$  are the rates of interfacial melting (or crystallization if negative). The four variables are  $V$ ,  $\phi$ ,  $c$  and  $s$ .

In seeking the very simplest form of the model, we take  $\rho_s = \rho_l = \rho$  to be constant, whence it follows that  $V$  is constant, and the equations take the form

$$\begin{aligned} \frac{\partial}{\partial t}(\phi c) &= \frac{\Sigma \Gamma_2}{\rho}, \\ \frac{\partial}{\partial t}\{\phi (1-c)\} &= \frac{\Sigma \Gamma_1}{\rho}, \end{aligned}$$

$$\begin{aligned}\frac{\partial}{\partial t}\{(1-\phi)s\} &= -\frac{\Sigma \Gamma_2}{\rho}, \\ \frac{\partial}{\partial t}\{(1-\phi)(1-s)\} &= -\frac{\Sigma \Gamma_1}{\rho};\end{aligned}\quad (3.4)$$

These are now four equations for three unknowns but one is redundant, as adding them yields an identity. We can therefore dispense with the last equation. We follow [Rudge \*et al.\* \(2011\)](#) in taking the melt rates to be proportional to the interfacial free energy differences between solid and liquid components, thus

$$\Gamma_i = \frac{E_i \rho v_R \Delta \mu_i}{RT_0}, \quad (3.5)$$

where  $\Delta \mu_i$  is defined in (2.15),  $T_0$  and  $v_R$  are a reference temperature and a reference interfacial growth rate (velocity), so that the coefficients  $E_i$  are dimensionless. Using the subsequent definitions of the activity coefficients, we obtain

$$\Gamma_1 = \frac{\rho v_R E_1 T}{T_0} \ln \left[ \frac{(1-y)\gamma_1(y)}{(1-x)K_1(T)} \right], \quad \Gamma_2 = \frac{\rho v_R E_2 T}{T_0} \ln \left[ \frac{y\gamma_2(y)}{xK_2(T)} \right]. \quad (3.6)$$

It is convenient to define a dimensionless time scale  $t^*$  through the differential relation

$$dt^* = \frac{\Sigma v_R T dt}{T_0}. \quad (3.7)$$

The first and third equations in (3.4) yield the conservation law

$$\phi c + (1-\phi)s = c_0, \quad (3.8)$$

and with this the model reduces to the two equations

$$\begin{aligned}\frac{\partial}{\partial t^*} \left[ \left( \frac{c_0 - s}{c - s} \right) c \right] &= E_2 G_2(x, y), \\ \frac{\partial}{\partial t^*} \left[ \left( \frac{c_0 - s}{c - s} \right) (1 - c) \right] &= E_1 G_1(x, y),\end{aligned}\quad (3.9)$$

where, using (2.16),

$$G_1 = \ln \left[ \frac{(1-y)}{(1-x)K_1} \right] + \chi y^2, \quad G_2 = \ln \left[ \frac{y}{xK_2} \right] + \chi (1-y)^2. \quad (3.10)$$

Henceforward we will omit the asterisk on the dimensionless time. As we hoped, (3.9) is a pair of ordinary differential equations for the two concentrations  $c$  and  $s$ . The temperature  $T$  and the total mass fraction  $c_0$  of component 2 provide the parameters of the model, so that the phase diagram becomes also a map of this parameter space.

A comment on the meaning of this model is necessary. It provides a description analogous to that used for well-mixed chemical reactions, whose kinetics are commonly studied in this way before the effects of transport are added. A drawback in the case of phase change is that the processes of transport in the solid phase are so slow that the presumption of spatial homogeneity within the solid phase is not very useful. However, this difficulty presents itself also in more general transport models. It does not matter if we consider crystallization, since it is only the average concentrations which matter. In the case of melting, it does not matter either if the crystals are homogeneous. It is only if melting and re-freezing occur in the solution of (3.9) that the crystallization history becomes important. With this proviso, we persevere in our analysis.

For simplicity, we will take equal molecular weights,  $M_1 = M_2$ , so that  $c = x$ ,  $s = y$ . We also define

$$X = \left( \frac{c_0 - s}{c - s} \right) c, \quad Y = \left( \frac{c_0 - s}{c - s} \right) (1 - c), \quad (3.11)$$

with inverse

$$c = x = \frac{X}{X + Y}, \quad s = y = \frac{c_0 - X}{1 - (X + Y)}, \quad (3.12)$$

and the model is

$$\begin{aligned} \dot{X} &= E_2 G_2(x, y), \\ \dot{Y} &= E_1 G_1(x, y), \end{aligned} \quad (3.13)$$

where the overdot indicates differentiation with respect to (dimensionless) time.

### 3.1 Phase plane dynamics

We have solved the model (3.13) numerically, and reconstructed the phase diagram of Fig. 6, as shown in Fig. 7. We need to provide values of  $T$  and  $c_0$ , and initial values for  $X$  and  $Y$ . (3.8) then gives the porosity. In practice, it is more physically sensible to provide the initial porosity  $\phi_0$  and the initial concentrations  $x_0$  and  $y_0$ , and then use these to provide the values for  $c_0$ ,  $X(0)$  and  $Y(0)$ . In practice, what we have done is choose  $\phi_0 = 0.5$  in all cases, and  $x_0 = y_0 = c_0$ .

The results of the numerical solutions are shown in Fig. 7. Referring to Fig. 6, initial values at  $b$  lead to  $\phi = 1$ , and initial values in  $g$  lead to  $\phi = 0$ . Initial points  $a$  and  $c$  between the liquidus and solidus curves (indicated by unfilled circles in Fig. 7) yield values of  $\phi \in (0, 1)$ , and the solid and liquid concentrations approach the solidus and liquidus curves. The approach in all case appears to be monotonic, including in the vicinity of the eutectic point  $e$ , so that the fixed points appear to be stable nodes. This conclusion will be confirmed later.

Numerically, this means that the two eigenvalues of the community matrix of the linearized system are negative. Because both  $x$  and  $y$  (and therefore also  $X$  and  $Y$ ) have turning points at the eutectic point (in Fig. 6 or 7), one of these eigenvalues must become equal to zero at the eutectic point. In general, we might expect it to pass through zero, but this is not the case. The explanation is that the model is essentially symmetric under the transformation  $x, y, c_0 \rightarrow 1 - x, 1 - y, 1 - c_0$  (and is precisely so

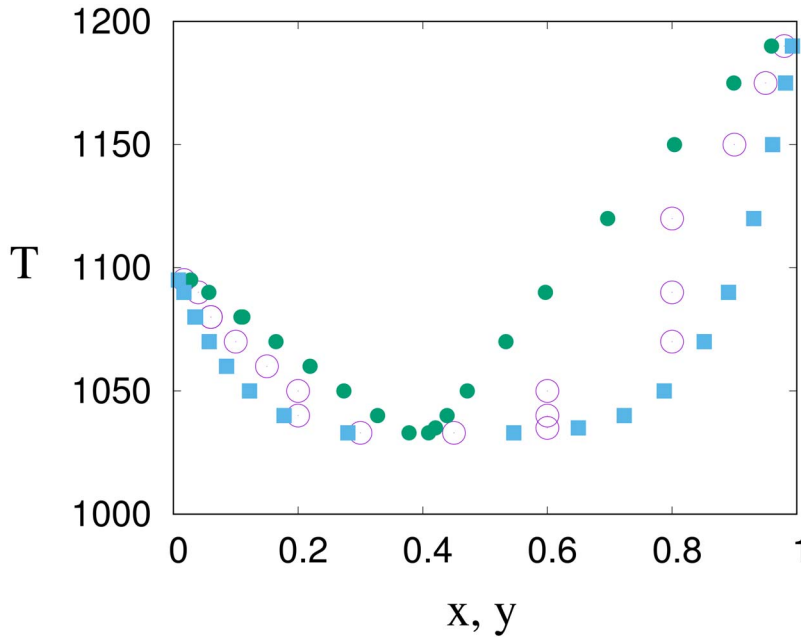


FIG. 7. The phase diagram in Fig. 6, but now obtained by numerically solving the pair of equations (3.13). The unfilled circles represent the values of  $T$  and  $c_0$  used.

if  $E_1 = E_2$ ,  $K_1 = K_2$ ), so that the two branches are both stable. The symmetry is associated with a pitchfork bifurcation (the ‘rod’ of the pitchfork being the solid solution below the eutectic temperature).

### 3.2 Solid unmixing

We now turn to the more complicated situation shown in Fig. 4, redrawn in Fig. 8 to show the possibly accessible parts of the phase diagram. Solid state unmixing causes the liquidus curves to cross each other, and we do now expect the dashed portions of the solidus and liquidus curves to be unstable (via saddle-node bifurcations). The solvus curves shown provide the eventual stable solid phases, but it is no longer obvious why the liquidus phases should not remain stable below the eutectic point.

In order to study this, we build a dynamic model similar to that discussed above. The complication is now that we need to deal explicitly with the formation of the eutectic solid phase, because below the unmixing temperature  $T_V$ , the solid state free energy  $G_S$  in (2.24) is  $W$ -shaped, having two minima either side of a central unstable maximum. We need therefore to address the issue of solid phase composition, which was not of concern in the earlier model, where the solid phase was taken to be homogeneous.

In a eutectic solid, solids of two different compositions crystallize simultaneously, and so we will have two separate crystal fractions having volume fractions  $\phi_A$  and  $\phi_B$ , specific surface areas  $\Sigma_A$  and  $\Sigma_B$  in contact with liquid, with corresponding mole fractions of component 1 of  $y_A$  and  $y_B$ . In addition there may be (certainly in a metal alloy, and always on complete solidification) a specific surface area  $\Sigma_S$  between the two solid phases. Issues of interfacial wetting occur here due to surface energy considerations, but for simplicity will be ignored. We will have the interphase free energy differences

$$\Delta\mu_i^C = RTG_i(x, y_C), \quad i = 1, 2, \quad C = A, B, \quad (3.14)$$

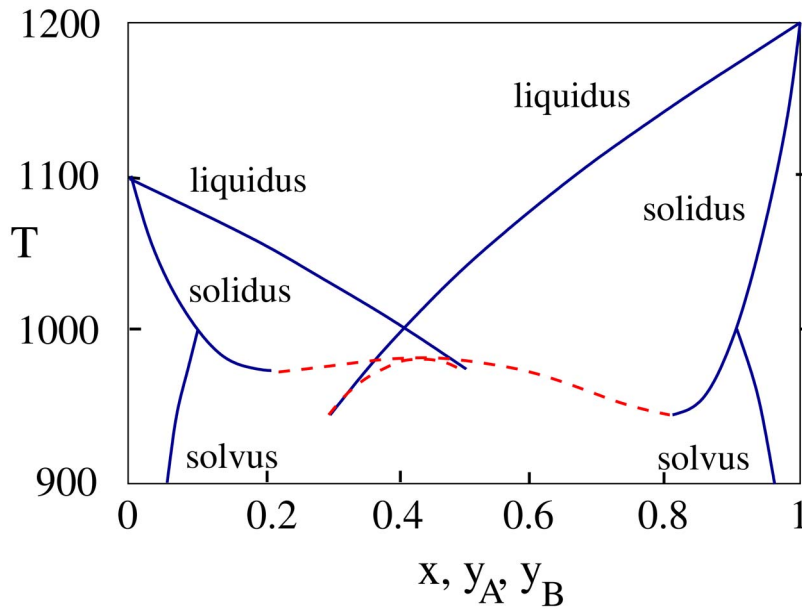


FIG. 8. The solidus and liquidus curves of Fig. 5; the presumably unstable branches caused by reversal of direction of the steady states as  $T$  varies are indicated by the red dashed lines. The solvus curves are the symmetric versions obtained from (2.22), with  $H_{21} = 0$ .

If  $c$ ,  $s_A$  and  $s_B$  are the concentrations of component 1 in liquid and solids  $A$  and  $B$ , then the conservation laws for the variables analogous to (3.3) are given by

$$\begin{aligned}
 \frac{\partial}{\partial t}(\rho_l \phi c V) &= V(\Sigma_A \Gamma_2^A + \Sigma_B \Gamma_2^B), \\
 \frac{\partial}{\partial t}\{\rho_l \phi (1 - c) V\} &= V(\Sigma_A \Gamma_1^A + \Sigma_B \Gamma_1^B), \\
 \frac{\partial}{\partial t}\{\rho_A \phi_A s_A V\} &= -V \Sigma_A \Gamma_2^A, \\
 \frac{\partial}{\partial t}\{\rho_B \phi_B s_B V\} &= -V \Sigma_B \Gamma_2^B, \\
 \frac{\partial}{\partial t}\{\rho_A \phi_A (1 - s_A) V\} &= -V \Sigma_A \Gamma_1^A, \\
 \frac{\partial}{\partial t}\{\rho_B \phi_B (1 - s_B) V\} &= -V \Sigma_B \Gamma_1^B.
 \end{aligned} \tag{3.15}$$

These are six equations for the seven variables  $\phi$ ,  $\phi_A$ ,  $\phi_B$ ,  $V$ ,  $c$ ,  $s_A$  and  $s_B$ ; the extra equation needed is

$$\phi + \phi_A + \phi_B = 1. \tag{3.16}$$

As earlier, we will assume that  $\rho_l = \rho_A = \rho_B = \rho$ , whence it follows that  $V$  is constant, and we assume equal molecular weights, so that  $x = c$ ,  $s_A = y_A$ ,  $s_B = y_B$ . We take the interfacial source terms to be

$$\Gamma_i^C = \frac{\rho v_R E_i \Delta \mu_i^C}{RT_0}, \quad i = 1, 2, \quad C = A, B. \quad (3.17)$$

We will also assume that

$$\Sigma_A = \frac{\phi_A \Sigma}{1 - \phi}, \quad \Sigma_B = \frac{\phi_B \Sigma}{1 - \phi}; \quad (3.18)$$

then, rescaling time in a similar fashion to that used earlier in (3.7),

$$d\tilde{t} = \frac{dt^*}{1 - \phi} = \frac{\Sigma v_R T dt}{(1 - \phi) T_0}, \quad (3.19)$$

and dropping the overtilde, we obtain the (dimensionless) set

$$\begin{aligned} (\phi x)_t &= \phi_A g_2^A + \phi_B g_2^B, \\ \{\phi(1 - x)\}_t &= \phi_A g_1^A + \phi_B g_1^B, \\ (\phi_A y_A)_t &= -\phi_A g_2^A, \\ (\phi_B y_B)_t &= -\phi_B g_2^B, \\ \{\phi_A(1 - y_A)\}_t &= -\phi_A g_1^A, \\ \{\phi_B(1 - y_B)\}_t &= -\phi_B g_1^B, \end{aligned} \quad (3.20)$$

where

$$g_i^C = E_i G_i(x, y_C). \quad (3.21)$$

These equations generalize (3.4), and must reduce to them if  $y_A = y_B$ . The equations (3.20) have the conservation law

$$\phi x + \phi_A y_A + \phi_B y_B = c_0, \quad (3.22)$$

as well as (3.16), so that the system is actually of fourth order. There appears to be no numerical advantage in reducing it in this way, and we have solved the sixth-order system directly, using the conservation laws as a simple check on the numerical method. In order to write it in an explicit form, analogous to (3.13), we define

$$X = \phi x, \quad Y = \phi(1 - x), \quad Z_A = \phi_A y_A, \quad Z_B = \phi_B y_B, \quad (3.23)$$

and the equations have the form

$$\begin{aligned}
 \dot{X} &= \phi_A g_2^A + \phi_B g_2^B, \\
 \dot{Y} &= \phi_A g_1^A + \phi_B g_1^B, \\
 \dot{Z}_A &= -\phi_A g_2^A, \\
 \dot{Z}_B &= -\phi_B g_2^B, \\
 \dot{\phi}_A &= -\phi_A (g_1^A + g_2^A), \\
 \dot{\phi}_B &= -\phi_B (g_1^B + g_2^B),
 \end{aligned} \tag{3.24}$$

where the right-hand sides also depend on  $x$ ,  $y_A$  and  $y_B$ , which are defined by

$$x = \frac{X}{X+Y}, \quad y_A = \frac{Z_A}{\phi_A}, \quad y_B = \frac{Z_B}{\phi_B}, \tag{3.25}$$

and the conservation law (3.22) is simply

$$X + Z_A + Z_B = c_0. \tag{3.26}$$

The model (3.24) provides six equations for the variables  $X$ ,  $Y$ ,  $Z_A$ ,  $Z_B$ ,  $\phi_A$ ,  $\phi_B$ . The functions  $g_i^C$  are defined in (3.21) and (3.10), in terms of the subsidiary quantities  $x$ ,  $y_A$ ,  $y_B$  defined in (3.25),  $\gamma_i$  defined in (2.16) and  $K_i$ , defined in (2.11), while  $\chi$  in the definitions of  $\gamma_i$  is defined in (2.17). We note that the coefficient  $H_{21}$ , which appeared in the discussion of solid phase equilibrium (see (2.22)), is absent from the model above. As already mentioned, the reason for this is that we have neglected to include intra-solid solid-state diffusion in the model, because the resultant approach to equilibrium (due to solid-solid interfacial free energy differences) may be very slow. This is likely to be the case in magma crystallization for example, where crystals of different compositions may grow in isolation, surrounded by liquid, with the approach to the solvus concentrations in the solid taking a very long time. In practice, we terminate the computations if either  $\phi$  or  $1 - \phi$  becomes less than  $10^{-3}$ , as the numerical method (fourth-order Runge–Kutta) breaks down in these limits. The value of the threshold (here  $10^{-3}$ ) depends on the step size used, here  $10^{-4}$ .

Figure 9 shows the equilibrium solutions corresponding to Fig. 8, obtained by solving (3.24) numerically until a steady state is obtained. It shows the states obtained as the solidus and liquidus curves in which the final state has  $0 < \phi < 1$ , i.e. coexisting solid and liquid. Of note is that the continuations of the states below the eutectic point remain stable, only disappearing as expected in a saddle-node bifurcation when the solidus curves reach their minima.

This seems surprising, as we might expect that initial states below the eutectic point in Fig. 8 would lead to solidification. To examine this, we have studied the evolution of initial conditions in the vicinity of the eutectic point, which is approximately at  $T = 1,001$  K,  $c_0 = 0.4$ . The result of this is shown in Fig. 10. The figure appends to the solidus and liquidus curves of Fig. 9 a curve of filled diamonds, which represents a boundary separating initial conditions (and thus also parameter values) which lead to combined solid/liquid equilibrium (above the curve) or total solidification (below the curve). To be clear,



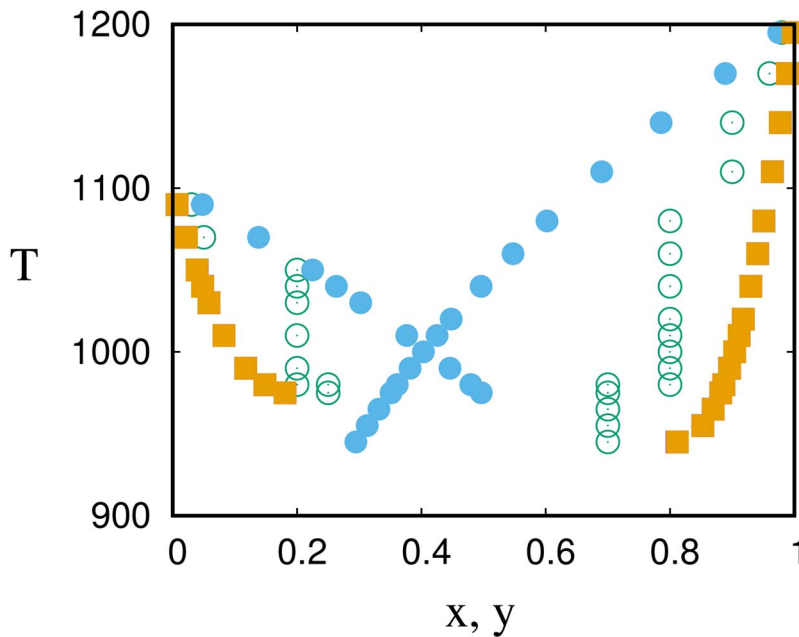


FIG. 9. The computed phase diagram corresponding to Fig. 8, obtained by solving (3.24) to its steady state, using parameters as in Fig. 4, and with  $E_1 = 0.5$ ,  $E_2 = 1$ . Similarly to Fig. 7, initial values of  $T$  and  $c_0$  are shown as open circles, with the resultant liquidus and solidus concentrations at the same temperatures indicated by filled circles and filled squares, respectively. In all the cases shown, the initial points lie between liquidus and solidus, and the final state has both solid and liquid ( $0 < \phi < 1$ ) present, and the two values of  $y_A$  and  $y_B$  are equal, even though they are unequal to begin with. Only when complete solidification occurs do we find  $y_A \neq y_B$ .

the solidus and liquidus curves in Fig. 9 (or Fig. 10) represent the final solid/liquid concentrations when the parameter values are set at the open circles in  $(c_0, T)$  space. The curve of filled diamonds in Fig. 10 appears to be a bifurcation curve in the  $(c_0, T)$  parameter space. This phase space diagram is confusing because it represents both the parameter space and the emerging steady states. It needs to be borne in mind that while the parameter space is indeed two-dimensional, the steady states represent a projection of the four-dimensional phase space described by  $(x, y_A, y_B, \phi)$ , for example, and in particular, the initial conditions for these four variables are not shown.

We need to elaborate our discussion of the four-dimensional phase space. Depending on our location in the two-dimensional  $(c_0, T)$  parameter space, one of three things can happen:  $\phi \rightarrow 0$  (solidification),  $\phi \rightarrow 1$  (melting) or  $\phi$  remains between 0 and 1 (mixed phase). In the latter case, the solutions always appear to approach a stable steady state. In such a steady state, the four quantities  $g_i^C \rightarrow 0$ , and because these are functions only of  $x$ ,  $y_A$  and  $y_B$  (at fixed  $T$ ), equilibrium generally requires  $y_A = y_B$ . (The exception is at the eutectic point.) This is why in Fig. 9, for example, the horizontal axis is only labelled  $x, y$ , rather than  $x, y_A, y_B$ . The mixed phase equilibria thus apparently lie in a three-dimensional subspace of the four-dimensional phase space. The equilibria are then defined by the solidus and liquidus concentrations as shown, with the third variable  $\phi$  not shown. However, this is not necessary, since if  $y_A = y_B = y$ , the conservation condition (3.26) then implies  $\phi \equiv \frac{c_0 - y}{x - y}$ , so that the equilibria actually lie on a two-dimensional surface.

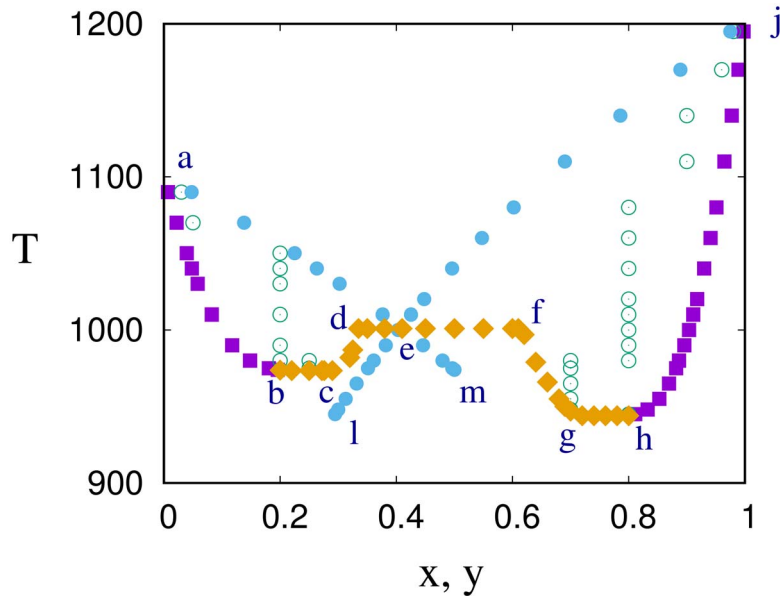


FIG. 10. Phase diagram as in Fig. 9, but with the addition of filled diamonds, which represent the boundary between states which solidify and states which maintain both solid and liquid phases (mixed-phase states).

These equilibria are those shown in Fig. 8, which suggested that the equilibria corresponding to the red dashed lines would be unstable, as indeed they are. If there is no stable mixed phase steady state, either  $\phi \rightarrow 0$  or  $\phi \rightarrow 1$  (in finite time).

For visualization purposes, think of the phase space as three-dimensional, with natural boundaries like a cube. The dynamics of the model then allow trajectories to reach the boundaries but not pass through. Once a trajectory reaches the boundary, it remains there and the dynamics would then in general follow lower dimensional dynamics on the boundary. Such a boundary could be expected to have a dimension one lower than the phase space, but in our case, the boundary where  $\phi = 0$  is actually two dimensions lower (because both  $X$  and  $Y \rightarrow 0$  as  $\phi \rightarrow 0$ ). In the case  $\phi \rightarrow 1$ , the boundary is actually a point, since then  $X \rightarrow c_0$ ,  $Y \rightarrow 1 - c_0$ ,  $\phi_A, \phi_B, Z_A, Z_B \rightarrow 0$ . In general, in the case  $\phi \rightarrow 0$ , we would have further evolution of  $y_A$  and  $y_B$  towards the solvus concentrations, but as mentioned above, that has been excluded from the model (3.24) (which is also why the corresponding values of  $y_A$  and  $y_B$  are excluded from Fig. 10).

As far as can be judged numerically, the curve of filled diamonds in Fig. 10 consists of three horizontal portions, one ( $def$ ) through the eutectic, and two ( $bc$  and  $gh$ ) tangent to both branches of the solidus curves at their minima. These are joined by the branches  $cd$  and  $fg$ , which appear to have non-zero slopes at the junctions with the horizontal parts. This provides some numerical justification for the otherwise fictional horizontal line in Fig. 1. In order to begin to understand Fig. 10, we will first use the fact that away from the eutectic point, steady mixed phase states have  $y_A = y_B$ , and if we look for particular solutions having this symmetry, the model reduces back to the two-dimensional system described earlier.

### 3.3 The two-dimensional phase plane

The reduction of (3.20) to two-dimensional form uses the fact that a particular solution is to take  $y_A = y_B = y$ , say, in which case also  $\phi = \frac{c_0 - y}{x - y}$ . The intersection of these two hyper-surfaces provide a four-dimensional subspace of the six-dimensional phase space which in reality can be taken to be three-dimensional in view of (3.16). The conservation law (3.22) then means that the three-dimensional phase space is foliated into a family of invariant two-dimensional subspaces, similar to constant energy hyper-surfaces in Hamiltonian systems. The reduction of the system to two dimensions leads to

$$\begin{aligned}\phi \dot{x} &= -xE_1 G_1 + (1-x)E_2 G_2, \\ (1-\phi)\dot{y} &= yE_1 G_1 - (1-y)E_2 G_2\end{aligned}\quad (3.27)$$

(equivalent to (3.13)), in which

$$\phi = \frac{c_0 - y}{x - y}, \quad 1 - \phi = \frac{x - c_0}{x - y}, \quad (3.28)$$

and  $G_1(x, y)$  and  $G_2(x, y)$  are given by (3.10). In writing (3.27), we have absorbed a factor  $1 - \phi$  into the timescale  $\tilde{t}$  by defining a new time by  $d\tilde{t} = (1 - \phi) dt$ , which of course returns us to the original time scale for the two-dimensional system. The fixed points of the system are given by pairs  $(x, y)$  satisfying  $G_1 = G_2 = 0$ , as shown in Fig. 8. Linearization at a fixed point leads to the equation  $\dot{\mathbf{w}} = M\mathbf{w}$  for the perturbation  $\mathbf{w}$ , and the stability of the fixed point is determined by the trace and determinant of the community matrix  $M$ . Using the definitions of the fixed points, we determine

$$\begin{aligned}\text{tr } M &= -E_1 \left[ \frac{1}{\phi} \frac{x}{(1-x)} + \frac{1}{(1-\phi)} \frac{y}{(1-y)} + \frac{2}{(1-\phi)} \ln \left\{ \frac{1-y}{K_1(1-x)} \right\} \right] \\ &\quad - E_2 \left[ \frac{1}{\phi} \frac{(1-x)}{x} + \frac{1}{(1-\phi)} \frac{(1-y)}{y} + \frac{2}{(1-\phi)} \ln \left\{ \frac{y}{K_2 x} \right\} \right],\end{aligned}\quad (3.29)$$

and

$$\det M = \frac{E_1 E_2 (x-y)^2}{\phi(1-\phi)xy(1-x)(1-y)} [1 - 2\chi y(1-y)]. \quad (3.30)$$

It seems possible that  $\text{tr } M > 0$  if  $K_1$  or  $K_2$  is large enough, but for all the calculations with our present choice of parameters, we find  $\text{tr } M < 0$  (and actually  $\text{tr } M < -2\sqrt{\det M}$ , so that  $A$  is a node). If  $\chi$  is large, an analytic determination is possible, which confirms this.

Figure 11 shows the numerically computed phase portrait for the parameter choice  $T = 965$  K,  $c_0 = 0.55$ . This is at a point approximately at the letter  $m$  in Fig. 10, where there are two fixed points (see Fig. 8) at approximately  $x = 0.3317, y = 0.8694$ , which is a stable node and marked  $A$ , and  $x = 0.3398, y = 0.6524$ , which is a saddle (it is on the red dashed curves in Fig. 8) and marked  $B$  in Fig. 11. The phase space is restricted to the two rectangles  $x < c_0, y > c_0$  and  $x > c_0, y < c_0$ , as these are where  $0 < \phi < 1$ . If a trajectory reaches  $x = c_0$ , then  $\phi = 1$  there (unless also  $y = c_0$ ), and

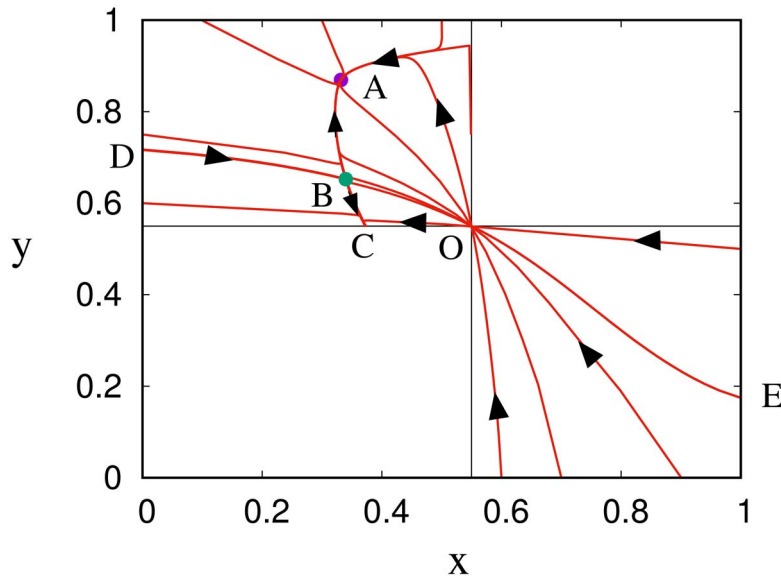


FIG. 11. Phase portrait for (3.27) at parameter values  $T = 965$  K,  $c_0 = 0.55$ .  $DB$  (actually two curves) is approximately the left stable separatrix to the saddle  $B$ , whereas the two curves emanating from  $E$  approximate the right separatrix

equivalently  $\phi = 0$  (solidification) at  $y = c_0$ . We see that most trajectories, but not all, reach the stable mixed phase state  $A$ , but initial states below  $DO$  in the left upper quadrant, or above  $EO$  in the right lower quadrant, will reach  $y = c_0$  and thus solidify.

Without indulging ourselves, it is not difficult by consideration of Fig. 8 to describe the resulting phase planes as  $T$  increases at this value of  $c_0$ . At higher  $T$ , a second saddle appears, but in the lower right quadrant. As  $T$  increases further, these two saddles coalesce (at  $x = y = c_0$ ) and disappear, leaving only the stable node; an example of the consequent phase plane is shown in Fig. 12, at a temperature  $T = 995$  K which is still below the eutectic; but in this two-dimensional reduction, the mixed-phase state is globally stable.

### 3.4 The four-dimensional phase space

The preceding discussion provides us with a tentative explanation for the ‘bifurcation’ curve in Fig. 10. In computing those results (in the four-dimensional model), we took a particular choice of initial values consistent with an initial mixed-phase state, and this choice depended on  $c_0$  and  $T$ . This corresponds to selecting a curve of initial conditions in the phase space. By analogy, if we choose a curve of initial values in Fig. 11 which crosses the stable separatrix of  $B$ , we will find some solutions tend to the mixed-phase state  $B$ , and others tend to complete solidification at  $C$ .

The key in Fig. 11 to the differing outcomes depending on initial conditions is the presence of the saddle, whose stable separatrices partition the two-dimensional phase space. Once the saddle disappears, the mixed phase state becomes globally stable, as in Fig. 12. A similar explanation is less easy to carry out (or visualize) in the full four-dimensional phase space. However, above  $T \approx 980$  K, the two saddles coalesce and disappear, and we can at least investigate the stability of the mixed phase steady state in the four-dimensional phase space.

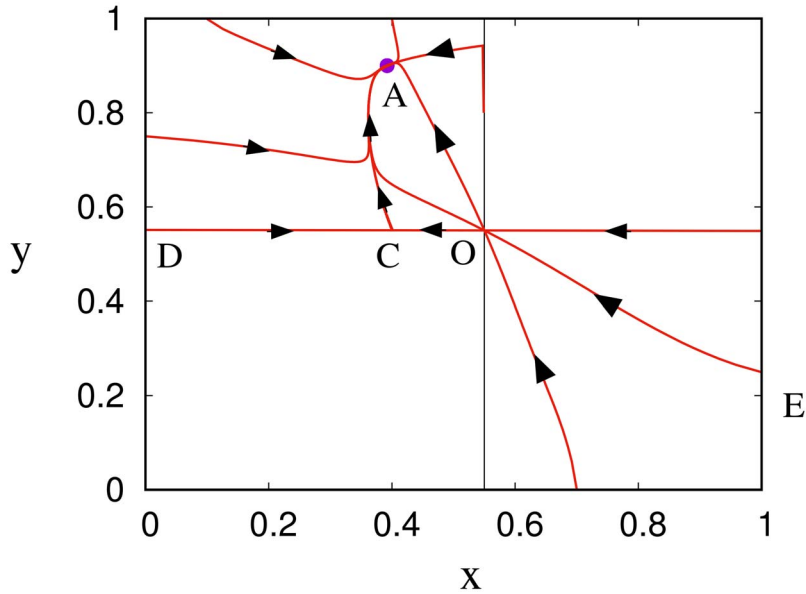


FIG. 12. Phase portrait for (3.27) at parameter values  $T = 995$  K,  $c_0 = 0.55$ . The saddle point in Fig. 11 has disappeared, and the mixed-phase state A is globally stable, in this two-dimensional model.

We can reduce the system (3.20) to the following set for the variables  $\phi$ ,  $x$ ,  $y_A$  and  $y_B$ :

$$\begin{aligned}\dot{\phi} &= \phi_A(g_1^A + g_2^A) + \phi_B(g_1^B + g_2^B), \\ \phi\dot{x} &= \phi_A[-xg_1^A + (1-x)g_2^A] + \phi_B[-xg_1^B + (1-x)g_2^B], \\ \dot{y}_A &= y_Ag_1^A - (1-y_A)g_2^A, \\ \dot{y}_B &= y_Bg_1^B - (1-y_B)g_2^B,\end{aligned}\tag{3.31}$$

where

$$\phi_A = \frac{y_B - c_0 + \phi(x - y_B)}{y_B - y_A}, \quad \phi_B = \frac{c_0 - y_A - \phi(x - y_A)}{y_B - y_A}.\tag{3.32}$$

As earlier, we linearize about the mixed phase steady state in which  $y_A = y_B = y$ . Denoting the perturbations by capitals (and the steady state quantities by lower cases), we find that the perturbation vector  $\mathbf{w} = (\Phi, X, Y_A, Y_B)^T$  satisfies the equation

$$\dot{\mathbf{w}} = L\mathbf{w}, \quad L = \begin{pmatrix} 0 & (\phi_A + \phi_B)p(x) & \phi_A p(y)L(y) & \phi_B p(y)L(y) \\ 0 & A & B & C \\ 0 & F & G & 0 \\ 0 & F & 0 & G \end{pmatrix},\tag{3.33}$$

where

$$A = -\frac{(1-\phi)}{\phi} \frac{f(x)}{x(1-x)}, \quad B = -\frac{\phi_A}{\phi} \frac{L(y)h(x,y)}{y(1-y)}, \quad C = -\frac{\phi_B}{\phi} \frac{L(y)h(x,y)}{y(1-y)},$$

$$F = \frac{h(x,y)}{x(1-x)}, \quad G = \frac{L(y)f(y)}{y(1-y)}, \quad (3.34)$$

and

$$p(x) = \frac{E_1x - E_2(1-x)}{x(1-x)}, \quad L(y) = -1 + 2\chi y(1-y),$$

$$h(x,y) = E_1xy + E_2(1-x)(1-y), \quad f(x) = h(x,x). \quad (3.35)$$

There is a constant solution  $\mathbf{w} = (1, 0, 0, 0)^T$ , which can be discounted if  $c_0$  is held fixed, because the conservation laws imply

$$(x-y)\Phi + \phi X + \phi_A Y_A + \phi_B Y_B = 0; \quad (3.36)$$

the uncoupled vector  $\mathbf{W} = (X, Y_A, Y_B)^T$  then satisfies  $\dot{\mathbf{W}} = M\mathbf{W}$ , where  $M$  is the first cofactor in  $L$ . Solutions are  $\propto e^{\lambda t}$ , where the eigenvalues  $\lambda$  are given by

$$\lambda = G, \quad \lambda^2 - T_r \lambda + D = 0, \quad (3.37)$$

in which

$$T_r = -\frac{(1-\phi)}{\phi} \frac{f(x)}{x(1-x)} + \frac{L(y)f(y)}{y(1-y)}, \quad D = -\frac{(1-\phi)}{\phi} \frac{E_1 E_2 (x-y)^2 L(y)}{xy(1-x)(1-y)}. \quad (3.38)$$

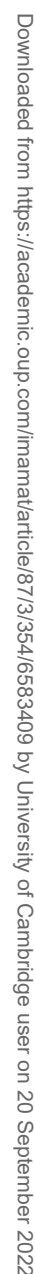
If  $L(y) < 0$ , which is the case on the stable parts of the solidus curve (the undashed parts in Fig. 8), it is straightforward to show that all three roots are real and negative (as we intimated in the two-dimensional case earlier). The mixed-phase steady state is thus linearly stable, but its stable manifold may only be three-dimensional. It may not be globally stable, and some trajectories may reach  $\phi = 0$ , and thus form a solid.

**3.4.1 Solidification.** For solidification to be possible, we require

$$\{\dot{\phi}x\} < 0 \quad \text{and} \quad \{\dot{\phi}(1-x)\} < 0 \quad \text{when} \quad \phi = 0, \quad (3.39)$$

and thus also when  $\phi\dot{x} = 0$ . Solidification is thus possible if

$$\phi_A g_1^A + \phi_B g_1^B < 0, \quad \phi_A g_2^A + \phi_B g_2^B < 0, \quad (3.40)$$



when also

Using the definitions of  $g_i^C$ , we find that (3.40) implies

where

These bounds and the computed  $x$  values for the filled gold diamonds shown in Fig. 10 are shown in Fig. 13, and clearly indicate that for eventual solidification, the liquid composition ends up between the two liquidus curves, when the temperature is below the eutectic. Despite a good deal of effort, I have not been able to demonstrate that solidification is impossible above the eutectic temperature. However, the matter is simply resolved in the strong unmixing limit of large  $\chi$  (which may commonly be appropriate).

3.4.2 *Strong unmixing.* If we denote the liquidus and solidus curves which emerge from  $x = y = 0$ ,  $T = T_1 = 1,100$  K in Fig. 8 as  $x_A(T)$  and  $y_A(T)$ , and the corresponding liquidus and solidus curves emerging from  $x = y = 1$ ,  $T = T_2 = 1,200$  K as  $x_B(T)$  and  $y_B(T)$ , then in the limit where  $\chi \gg 1$ , the equilibrium curves are given approximately by

$$x_A = 1 - \frac{1}{K_1}, \quad y_A = \delta K_2 x_A, \quad x_B = \frac{1}{K_2}, \quad y_B = 1 - \delta K_1 (1 - x_B), \quad (3.44)$$

where

$$\delta = e^{-\chi}. \quad (3.45)$$

This approximation is thus useful even for relatively moderate values of  $\chi$ , and corresponds to the formation of almost pure solids.

To describe the non-equilibrium growth in this situation, we define

$$y_A = \delta \eta_A, \quad y_B = 1 - \delta \eta_B, \quad (3.46)$$

and then the equations (3.31) can be written in the approximate form, using (3.10) and (3.21),

$$\begin{aligned} (\dot{\phi}x) &= E_2 \phi_A \ln \left( \frac{\eta_A}{K_2 x} \right) - E_2 \phi_B \ln(K_2 x), \\ \{\phi(1-x)\} &= -E_1 \phi_A \ln\{K_1(1-x)\} + E_1 \phi_B \ln \left[ \frac{\eta_B}{K_1(1-x)} \right], \\ \delta \dot{\eta}_A &= -E_2 \ln \left( \frac{\eta_A}{K_2 x} \right), \\ -\delta \dot{\eta}_B &= E_1 \ln \left[ \frac{\eta_B}{K_1(1-x)} \right], \end{aligned} \quad (3.47)$$

with algebraic error terms of  $O(\delta)$ . Here

$$\begin{aligned} \phi_A &\approx 1 - c_0 - \phi(1-x), \\ \phi_B &\approx c_0 - \phi x. \end{aligned} \quad (3.48)$$

The solidus concentrations rapidly approach equilibrium,

$$\eta_A \approx K_2 x, \quad \eta_B \approx K_1(1-x), \quad (3.49)$$

so that the system reduces to

$$\begin{aligned} (\dot{\phi}x) &= \phi_B g_2^B = -E_2 \phi_B \ln(K_2 x), \\ \{\phi(1-x)\} &= \phi_A g_1^A = -E_1 \phi_A \ln\{K_1(1-x)\}. \end{aligned} \quad (3.50)$$



It is now straightforward to see that above the eutectic and between the two liquidus curves, complete melting occurs, while below the eutectic and between the two liquidus curves, complete solidification occurs, consistent with Fig. 13. In the other two regions, to the right and left of the eutectic point, the sign of  $\dot{\phi}$  is uncertain, and in particular depends on the growth rate coefficients  $E_1$  and  $E_2$ . This is also consistent with the numerical results in Fig. 10.

#### 4. Discussion

Does any of this matter? For rapid growth rates, generally not. For a slowly cooling liquid, crystallization commences when the temperature reaches the liquidus, and as the temperature is reduced further, the liquid composition follows the liquidus down to the eutectic, and further cooling below this causes complete solidification, as in (3.50). However, if cooling is sufficiently rapid, or crystallization is sufficiently slow, it may be possible to remain on the solidus/liquidus below the eutectic temperature. This perhaps occurs during rapid quenching, and if the unmixing coefficient  $\chi$  is large, it will continue to temperatures well below the eutectic. In fact, approximation of the solidus at large  $\chi$  shows that the minimum  $b$  in Fig. 13 occurs when

$$y_A \approx \frac{1}{2\chi}, \quad K_2 \approx \frac{e^{\chi-1}}{2\chi} \quad (4.1)$$

(assuming also  $K_1 \gg 1$ ), and a steady mixed-phase solution is possible for temperatures above this.

This brings to mind the common observation that water can sometimes be supercooled without forming ice. A small vibration will then cause it to freeze. The usual explanation is that freezing is prevented by the absence of nucleation sites, because of the surface energy induced barrier to homogeneous nucleation. The present discussion provides an alternative interpretation, which is simply that (perhaps by rapid cooling at low impurity concentrations), a stable mixed phase state is obtained, which is however unstable to sufficiently large perturbations in the state space.

Where the theory of this paper may be important is in situations where the interfacial growth rate is comparable to the cooling rate; one such situation may occur in the crystallization of magma chambers, because the interfacial growth rates of silicate rocks are commonly very small (Dowty 1980).

#### 5. Conclusions

Motivated by the wish to understand the construction of and approach to equilibrium in the phase diagram of binary alloys, we have studied a representative model system which describes the non-equilibrium growth of crystals from a two-component mixture. Our study has illuminated the significance of the eutectic point, and shown that complete solidification will occur at the eutectic composition for temperatures below the eutectic temperature. But we have also shown that mixed-phase solid/liquid equilibria can exist in stable form below the eutectic temperature, which thus provides an explanation for observations of supercooled liquids which is distinct from (and perhaps preferable to) the usual one which involves the nucleation barrier.

Our results have little impact in situations where cooling is slow or interfacial growth rates are large, but they may have significance where these assumptions are invalid, one example of which may be in the crystallization of magma chambers.

## Acknowledgements

A.C.F. acknowledges the support of the Mathematics Applications Consortium for Science and Industry (www.macsi.ul.ie) funded by the Science Foundation Ireland mathematics grant 12/IA/1683.

## REFERENCES

- CAHN, J. W. & HILLIARD, J. E. (1958) Free energy of a non-uniform system. I. Interfacial free energy. *J. Chem. Phys.*, **28**, 258–267.
- DOWTY, E. (1980) Crystal growth and nucleation theory and the numerical simulation of igneous crystallisation. *Physics of magmatic processes* (R. B. HARGRAVES ed). Princeton, N. J: Princeton University Press, pp. 419–485.
- FLEMINGS, M. C. (1974) *Solidification processing*. New York: McGraw–Hill.
- FLORY, P. J. (1942) Thermodynamics of high polymer solutions. *J. Chem. Phys.*, **10**, 51–61.
- FOWLER, A. (2011) *Mathematical geoscience*. London: Springer-Verlag.
- KUHL, E. & SCHMID, D. W. (2007) Computational modeling of mineral unmixing and growth: an application of the Cahn–Hilliard equation. *Comput. Mech.*, **39**, 439–451.
- MAALØE, S. (1978) The origin of rhythmic layering. *Mineral. Mag.*, **42**, 337–345.
- MARGULES, M. (1895) Über die Zusammensetzung der gesättigten Dämpfe von Mischungen. *Sitzb. d. mathem.-naturw. Cl.*, **104**, 1,243–1,278.
- MCBIRNEY, A. R. (1984) *Igneous petrology*. San Francisco, CA: Freeman, Cooper and Co.
- MORSE, S. A. (1980) *Basalts and phase diagrams: an introduction to the quantitative use of phase diagrams in igneous petrology*. Berlin: Springer-Verlag.
- RUDGE, J. F., BERCOVICI, D. & SPIEGELMAN, M. (2011) Disequilibrium melting of a two phase multicomponent mantle. *Geophys. J. Int.*, **184**, 699–718.
- WAGER, L. R. & BROWN, G. M. (1968) *Layered igneous rocks*. Edinburgh: Oliver and Boyd.